TOMOGRAPHY RESEARCH ARTICLE

Pre-Labeling of Immune Cells in Normal Bone Marrow and Spleen for Subsequent Cell Tracking by MRI

Gabrielle M. Siegers[1], Shruti Krishnamoorthy[1,2], Laura E. Gonzalez-Lara[1], Catherine McFadden[1], Yuhua Chen[1], and Paula J. Foster[1,2]

[1]Imaging Research Laboratories, Robarts Research Institute, London, Ontario, Canada; and [2]Department of Medical Biophysics, Western University, London, Ontario, Canada

Corresponding Author:
Paula Foster, PhD
Imaging Research Laboratories, Robarts Research Institute, 1151 Richmond Street North, London Ontario, Canada, N6A 5B7
E-mail: pfoster@robarts.ca

Key Words: MRI, mice, iron, macrophage, inflammation

Abbreviations: 3D balanced steady-state free precession (bSSFP), complete Freund's adjuvant (CFA), experimental autoimmune encephalomyelitis (EAE), ethylenediaminetetraacetic acid (EDTA), forward scatter (FSC), hematoxylin & eosin (H&E), intravenous/intravenously (IV), micron-sized iron oxide particles (MPIO), magnetic resonance imaging (MRI), magnetic resonance (MR), multiple sclerosis (MS), mesenchymal stem cells (MSC), Perl's Prussian Blue (PPB), radio-frequency (RF), signal to noise ratio (SNR), superparamagnetic iron oxide nanoparticles (SPIO), side scatter (SSC), echo time (TE), repetition time (TR), ultra-small superparamagnetic iron oxide particles (USPIO)

ABSTRACT

Iron particles are intravenously (IV) administered to label cells in vivo during magnetic resonance imaging. This technique has been extensively used to monitor immune cells in the context of inflammatory diseases. Here, we have investigated whether resting immune cells can be labeled in vivo in healthy mice before disease onset or injury, thus allowing visualization of critical early cellular events. Using 1.5 T magnetic resonance imaging, we were able to detect signal loss in bone marrow, liver, and spleen as early as 1 hour after the IV injection of superparamagnetic iron oxide nanoparticles (Feridex; 80 to 120 nm in diameter) or larger micron-sized iron oxide particles (Bangs; 0.9 μm in diameter). Results were confirmed via histology. Further, flow cytometric analysis confirmed the presence of iron-labeled $CD19^+$ B cells, $CD3^+$ T cells, and $CD11b^+$ myeloid cells within the spleen and the bone marrow. Extending this work to a murine model of multiple sclerosis, we IV administered superparamagnetic iron oxide to healthy mice 1 week before inducing experimental autoimmune encephalomyelitis. Images acquired 1 week after the onset of hindlimb paralysis showed regions of signal hypointensity in the mouse brain that corresponded with iron-labeled macrophages. In summary, we show that resting immune cells in the healthy mouse liver, spleen, and bone marrow can be prelabeled with iron oxide nanoparticles. Furthermore, iron oxide preloading of immune cells in the reticuloendothelial system can be used to detect cellular infiltration in the brains of experimental autoimmune encephalomyelitis mice.

INTRODUCTION

Iron oxide nanoparticles have been extensively used to label immune cells in vivo for MRI-based tracking of cellular infiltration and inflammation in disease and injury (1–7). Iron particles are typically administered intravenously (IV) and are subsequently engulfed by macrophages in the reticuloendothelial system. MRI is then performed approximately 1 day after the IV injection of iron to visualize the accumulation of iron-labeled inflammatory cells at the sites of either injury or disease; this timeframe also permits clearance of intravascular iron.

The accumulation of iron-labeled cells results in an area of signal loss in magnetic resonance (MR) images by causing field inhomogeneities, which shorten T2 and T2*. Both ultrasmall superparamagnetic iron oxide (USPIO; ~10–30 nm) particles and standard superparamagnetic iron oxide (SPIO; ~30–120 nm) particles have been used to characterize inflammation in experimental autoimmune encephalomyelitis (EAE), a mouse model of multiple sclerosis (MS), whereby IV-administered iron particles were phagocytosed by macrophages and tracked to regions of active inflammation in the brain (2, 8, 9). Micron-sized iron oxide (MPIO) particles have also been used to image inflammation with MRI in models of organ rejection and myocardial infarction (10, 11). USPIO particles have been used this way to image inflammation in human patients with MS, atherosclerosis, stroke, myocardial infarction, and diabetes (12–18).

More recently, the concept of in vivo iron loading of resident immune cells in the bone marrow has been presented as a method by which cells can be prelabeled with iron to allow tracking of their subsequent migration. For example, Khurana et al preloaded preloaded macrophages with IV ferumoxytol before

ISSN 2379-1381 http://dx.doi.org/10.18383/j.tom.2016.00103

stem cell transplantation into osteochondral defects in rats. In this study, the USPIO particles were IV administered, and 48 hours later, both viable and apoptotic stem cells were transplanted. MRI performed 2 and 4 weeks later showed signal loss associated only with the apoptotic transplants, and histology confirmed the presence of greater numbers of iron-positive macrophages in the apoptotic transplant sites (15).

In this study, we investigate the potential for in vivo prelabeling of specific immune cell populations in the bone marrow and the spleen in healthy mice. An application of this cell-tracking approach for monitoring the accumulation of iron-labeled cells in EAE lesions in the mouse brain is also shown. Prelabeling immune cells with iron oxide particles in vivo may permit MRI monitoring of their mobilization and trafficking in response to disease states, without ex vivo manipulation, which could potentially lead to contamination or unanticipated/unwanted biological modification.

METHODOLOGY

Healthy Mice—In Vivo Iron Labeling Experiments

We used 8- to 11-week-old female C57Bl/6 mice (n = 39; Charles River Laboratories, Wilmington, Massachusetts) housed in pathogen-free conditions until use. The SPIO agent Feridex® was used (average diameter, 80-120 nm; Advanced Magnetic Industries, Massachusetts). The 2 fluorescently tagged MPIO particles used were Flash Red and Dragon Green (Bangs Laboratories Inc., Fishers, Indianapolis); their emission and excitation spectra are 620/690 and 500/580, respectively, and the average particle size was 0.9 μm.

All mice in this study were injected IV with either SPIO or MPIO particles at 30 mg of Fe/kg body weight via the tail vein in a total volume of 200 μL of saline or saline only (controls). Mice in group 1 were injected with either SPIO (n = 8) or MPIO particles (Flash Red Bangs Beads; n = 8). Iron-administered mice plus 4 control mice were subject to a prescan and imaged at 1 hour, 24 hours and 1 week after injection.

Mice in group 2 were injected with SPIO (n = 4), MPIO (n = 4), or saline (n = 2), and then sacrificed 24 hours after injection. Femurs and tibias were removed for histological analysis.

Mice in group 3 were injected with MPIO particles (Dragon Green Bangs Beads; n = 7) or saline (n = 2). Animals were sacrificed 24 hours after injection; the splenocytes and bone marrow cells were collected and analyzed for MPIO particle uptake using flow cytometry.

Mouse Model of Experimental Autoimmune Encephalomyelitis

SPIO particles were administered IV, as described above, to group 4 that comprised 10 healthy 6-week-old female C57Bl/6 mice. One week later, EAE was induced by subcutaneous injection of a mixture of 100 μg of synthetic myelin oligodendrocyte glycoprotein peptide 35-55, 0.050 mL of complete Freund's adjuvant, and 500 μg of irradiated mycobacterium tuberculosis. The type of iron particle and the timing of inducing EAE were chosen on the basis of the results from imaging of mice in group 1. Then, 0.1 mL of homogenate was injected in the flank of anesthetized mice. Pertussis toxin (500 ng) was administered intraperitoneally on day 0 and day 2 post disease immunization. A booster injection, in which incomplete Freund's adjuvant replaced complete Freund's adjuvant, was given 8 days later. The EAE mice were imaged the day after signs of hindlimb paralysis became evident (between days 12 and 16 after immunization) and 1 week later.

Magnetic Resonance Imaging

Mouse imaging was performed on a 3T GE Excite MR750 clinical MR system (General Electric, Mississauga, ON, Canada) using a custom-built insertable gradient coil. Whole-body images were acquired by positioning the mouse supine in a custom-built solenoidal mouse body radio-frequency (RF) coil (4 × 3 cm). Mouse brain images were acquired using a custom-built solenoidal mouse head RF coil (inner diameter of 1.5 cm). While scanning, mice were anesthetized using isoflurane gas (2% in oxygen), and normal body temperature was maintained by placing warm saline bags on either side of the coil. Images were generated using a 3-dimensional balanced steady-state free precession pulse sequence. For mouse body images, the parameters were as follows: repetition time (TR)/echo time (TE) = 4/2.7 milliseconds; flip angle = 30°; bandwidth = ±41 kHz; signal averages = 4; RF phase cycles = 4; slice thickness = 0.2 mm; and field of view = 6 cm, with a 300 × 300 matrix, resulting in 200 × 200 × 200 μm of isotropic resolution. Image acquisition took approximately 30 minutes per animal. For mouse brain images, the parameters were as follows: TR/TE = 8/4 milliseconds; flip angle = 40°; bandwidth = ±21 kHz; signal averages = 4; RF phase cycles = 4; slice thickness = 0.2 mm; and a field of view = 1.5, with a 150 × 150 matrix, resulting in 100 × 100 × 200 μm of resolution. Acquiring the images took approximately 35 minutes per animal.

MR images were analyzed using the OsiriX analysis program (Pixmeo, Switzerland). Signal-to-noise ratio (SNR) was calculated for the liver, spleen, muscle, lymph nodes, and bone marrow in each animal. Statistical analysis of the differences between SNR for images from SPIO- and MPIO-injected mice was conducted through a repeated measures analysis of variance, with a Tukey–Kramer multiple comparisons test for significance between the various time points. Differences were considered significant if $P < .05$.

Histopathology

Mice in groups 1 and 4 were perfused, and their brains, livers, and spleens were removed and prepared for histopathology. Tissues were paraffin embedded, and 5-μm sections were cut by a microtome. Slides were stained with hematoxylin & eosin and Perl's Prussian Blue (PPB) to verify the presence of iron. F4/80 was used to stain the brain tissue for macrophages. PPB-stained spleen sections were analyzed by counting the number of iron-positive white pulp regions in 10 random fields of view at 10× magnification. A total of 200 and 180 white pulp regions in MPIO- and SPIO-injected mice, respectively, were assessed for PPB positivity.

Bone Marrow Decalcification

Mice in group 2 were sacrificed by euthanyl overdose (180 mg/kg) 24 hours after IV iron injection. Tibias and femurs from each mouse were collected and fixed in 4% paraformaldehyde

for 24 hours. Bones were decalcified by immersion in a solution of 5% ethylenediaminetetraacetic acid (EDTA) for 1 week. Decalcified bones were then embedded in paraffin, and 2-μm sections were cut and placed onto microscope slides in alternating sections of 4 serial sections. Sections were stained with hematoxylin and eosin or PPB as described above. Representative bright-field images were collected and analyzed for iron content.

Flow Cytometry

Mice in group 3 (n = 9) were euthanized 24 hours after injection. The bone marrow and spleens were removed and placed in phosphate-buffered saline (PBS) + 1% fetal bovine serum (FBS) on ice. Splenic tissue was homogenized, and single-cell suspensions were created by mechanical disruption. The bone marrow was harvested by centrifugation, and then resuspended in 50 μL fluorescence-activated cell sorting (FACS) buffer ([FB]: PBS + 1% FBS + 2mM EDTA). Further, 4 mL ACK lysis buffer (0.155M NH_4Cl, 10mM $KHCO_3$, and 0.1mM Na_2EDTA in distilled H_2O) was added, and the cells were incubated for 10 minutes at room temperature with frequent vortexing. Then, 10 mL cold FB was added, cells were centrifuged (10 minutes, 400 g), supernatants were removed, and pellets were resuspended in 1 mL FB. Cells were counted and adjusted to 10×10^6 cells/mL in FB, and then blocked with normal goat serum (1:20, Sigma-Aldrich, St. Louis, Missouri) for 10 minutes on ice. Cells were washed in FB and either left unstained (unstained, secondary-only and isotype controls) or stained with the following primary antibodies for 30 minutes on ice: hamster anti-mouse CD3 biotin (1:100; a marker for T cells), anti-CD11b PE (1:800; a monocyte/macrophage marker), or anti-CD19 PerCPCy5.5 (1:2000, a marker for B cells). After washing, cells were resuspended in FB alone (unstained, anti-CD11b PE samples), FB-containing Streptavidin-APC (1:2000), or the isotype controls IgG2bk PE (1:800) or IgG2ak PerCPCy5.5 (1:2000) and incubated for 30 minutes on ice in the dark. Cells were washed and fixed in 200 μL FB containing 2% paraformaldehyde. The following day, flow cytometric acquisition was performed on a FACSCalibur (BD Biosciences, Mississauga, Ontario, Canada). All antibodies were purchased from BD Biosciences, Mississauga, Ontario, Canada. FlowJo© software (Tree Star Inc., Ashland, Oregon) was used to analyze the flow cytometric data.

RESULTS

MRI of Healthy Mouse Tissues

Figure 1 shows representative sagittal images of mice from group 1 before iron administration and at (A), 1 hour (B), 1 day (C), and 1 week (D) postinjection with either SPIO or MPIO. In the prescan image (Figure 1A, left and right), the femur (thigh bone, arrow) has a black outline and the bone marrow within appears gray. The spleen shows black speckles, and the liver is a uniform gray. This is expected because the spleen contains regions of red pulp where hemosiderin-laden macrophages that have phagocytosed old red blood cells reside; this iron causes some background signal loss.

After SPIO injection (Figure 1A, left), signal loss was evident in the bone marrow, liver, spleen, and some lymph nodes. Signal loss increased in the bone marrow between 1 hour (Figure 1B, left) and 1 day (Figure 1C, left), and this had not recovered to preinjection intensities by the 1-week time point (Figure 1D, left) in any tissue analyzed.

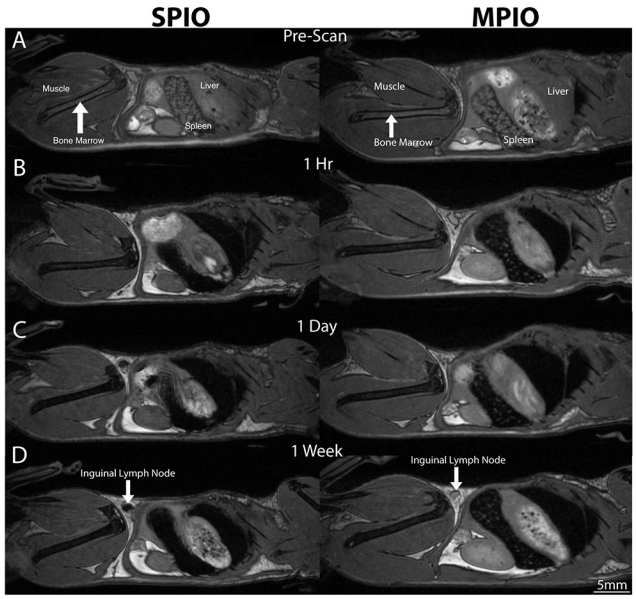

Figure 1. Sagittal balanced steady-state free precession whole-body images of SPIO-injected mice (left) and MPIO-injected mice (right) show normal signal aspect before injection (A) and signal loss in the liver, spleen, and bone marrow at 1 hour (B), 1 day (C), and 1 week (D) postinjection and in the inguinal lymph node for SPIO (D, white arrow).

After MPIO injection, signal loss was observed in the bone marrow, liver, and spleen at all time points (Figure 1, right side B–D) in all mice. As with SPIO, signal loss first appeared in images acquired at 1 hour (Figure 1B, right) after injection. The degree of signal loss in the bone marrow, spleen, and liver remained constant over time, with a greater degree of signal loss resulting from SPIO in the bone marrow, compared with that resulting from MPIO (compare left versus right). The greatest differences were evident in the spleen: those of SPIO-injected mice showed a complete signal void (Figure 1, left side B–D), whereas those from MPIO-injected mice still appeared speckled within (Figure 1, right side B–D).

In the images of the 4 SPIO-injected mice, 24 lymph nodes were visually assessed (pairs of inguinal, popliteal, and axillary nodes). Signal loss was observed within 14/24 nodes at 1 hour, 18/24 nodes at 24 hours, and 13/24 nodes at 1 week after injection (data not shown). The signal loss was not consistent in mice and was usually not uniform throughout the node (data not shown). Figure 2 shows the SNR measurements for the bone marrow, spleen, liver, and muscle over time in SPIO- and MPIO-injected mice. Analysis of the muscle surrounding the bone marrow revealed no visibly detectable change in the signal intensity after injection of either SPIO or MPIO (Figure 2D).

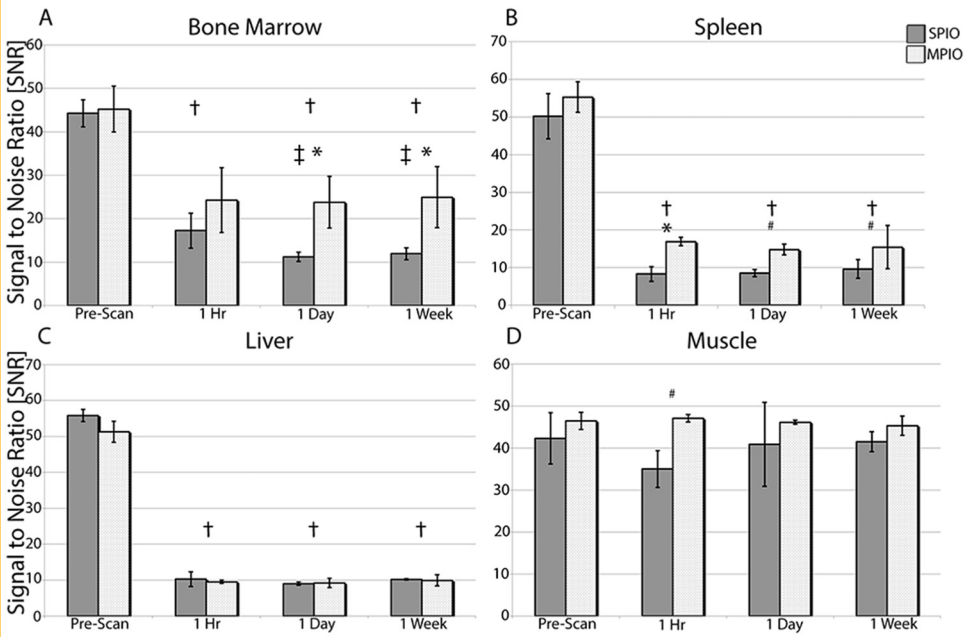

Figure 2. SNR measurements after IV SPIO and MPIO injections of the bone marrow (A), spleen (B), liver (C), and muscle (D).
$^{\dagger}P < .05$ denotes a significant difference between the prescan and other time points, $^{*}P < .01$ and $^{\#}P < .05$ denote a significant difference between MPIO and SPIO, respectively, and $^{\ddagger}P < .05$ denotes a significant difference in the SPIO SNR measurement compared to the 1-hour time point.

Histopathology of the Liver and Spleen

Histopathological analysis revealed iron-positive cells within the liver, spleen, and bone marrow of iron-injected mice and in the spleen of saline-injected mice. PPB staining for the spleens is shown in Figure 3. Iron, indicated by the blue color of PPB-stained cells, was observed in the spleens of all SPIO-injected mice (Figure 3A–C) or MPIO-injected mice (Figure 3D–F).

In SPIO-injected mice (Figure 3A–C), PPB staining was observed in the red pulp (Figure 3A, red pulp and box i), in the germinal center of the white pulp (Figure 3A, white pulp and box ii), and in the marginal zone located between the white pulp and the red pulp (Figure 3A, marginal zone outlined). In the spleens from MPIO-injected mice, PPB-stained cells were observed in the red pulp (Figure 3D, box iii is in the subcapsular red pulp)

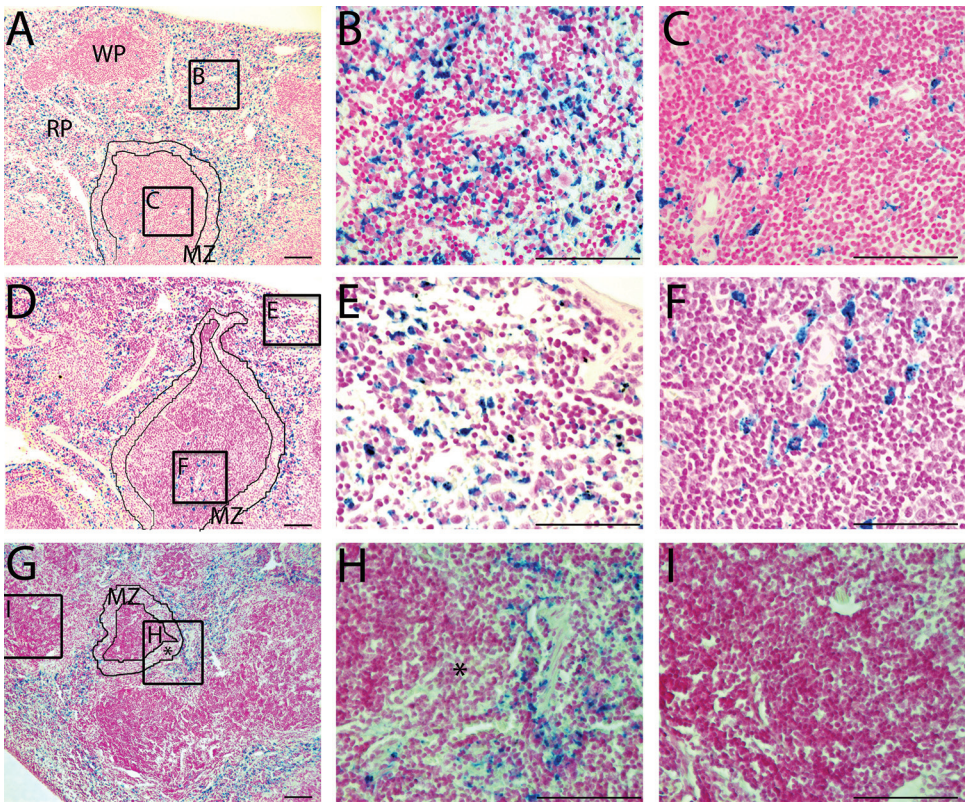

Figure 3. PPB-stained sections of the spleen reveal iron (blue) in the red pulp (RP), white pulp (WP), and marginal zone (MZ) areas of SPIO-injected mice (A, magnification 10×). At higher magnification (40×), iron-labeled cells are clearly observed in the red pulp (B) and in the white pulp (C). PPB+ areas are also present in the spleen of an MPIO-injected mouse (D), and, at higher magnifications, it can be observed that iron-labeled cells are located within the red pulp (E), and the subcapsular region of the white pulp (F). Control mice (G) have iron present only in the red pulp (H) but are PPB− in the white pulp (I) and in the marginal zone (*in G with a corresponding magnification in H). All scale bars = 100 μm.

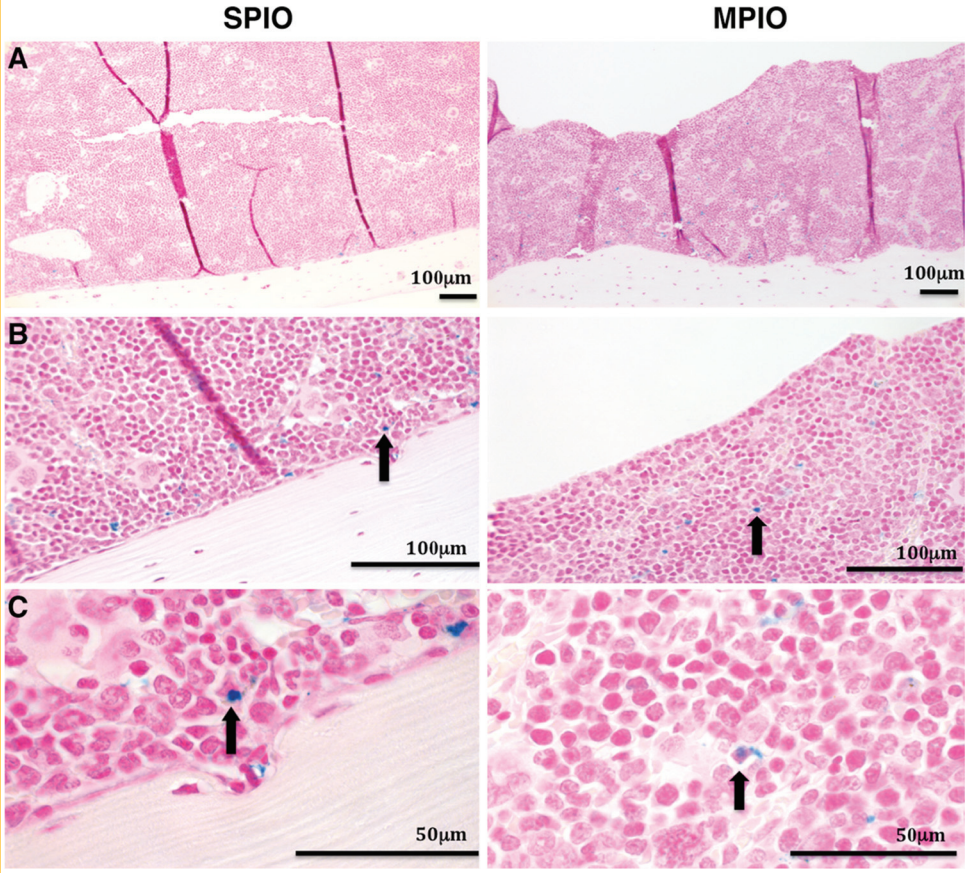

Figure 4. PPB-stained section of femurs from SPIO-injected mice (left) and MPIO-injected mice (right). The darker bone marrow, lined by lighter decalcified bone, contains cells labeled with iron (blue) as seen at 10× (A), and in greater detail at 40× (B), and 100× (C). Black arrows highlight PPB+ cells in B and C for SPIO (left) and MPIO (right), respectively.

and in the germinal center of the white pulp (Figure 3D, box iv) but, notably, not in the marginal zone. For both SPIO and MPIO, PPB staining observed within the white pulp was most often located in close proximity to the central arteries. Quantitative analysis of PPB-stained sections showed that 86% of the white pulp regions examined in the spleens of MPIO-injected mice and 99% of SPIO-injected mice contained iron-positive cells. In spleens from control mice (G-I), PPB staining was present only in the red pulp. The baseline PPB staining observed here was because of the presence of hemosiderin-laden macrophages, normally found in this region.

Decalcified samples of bone from SPIO-injected mice (Figure 4, left) and MPIO-injected mice (Figure 4, right) revealed iron-positive cells in the interior regions of the bone marrow tissue and along the periphery adjacent to the cortical bone. Samples collected from the control mice did not stain positive for iron (data not shown).

Flow Cytometry of the Bone Marrow and Spleen

To identify immune cells taking up injected MPIO in the bone marrow and spleens of healthy C57Bl/6 mice, we used antibodies that recognized the T-cell marker CD3, B-cell marker CD19, and the myeloid lineage marker CD11b to detect these cells via flow cytometry. Live cells were gated for lymphocytes, as well as for monocytes, neutrophils, and eosinophils (MNE) together. The MPIO uptake resulted in a considerable shift in side scatter (SSC) properties, thus gates-included events with high SSC and separation of MNE from one another were precluded (Figure 5, A and B, forward scatter versus SSC plots).

Figure 5A shows a representative example obtained for identification of T cells within the lymphocyte population and myeloid cells in the MNE-gated population in the spleen; Figure 5B shows the same for bone marrow. CD3 and CD11b expression were plotted against MPIO, and gates were set on the basis of the appropriate secondary-only or isotype controls (indicated, middle-column plots). In this representative mouse, 0.27% of live splenic lymphocytes were MPIO+ T cells, and 1.27% of live splenic MNE cells were both MPIO+ and $CD11b^+$. In the bone marrow, 0.39% of live lymphocytes were MPIO+ T cells and 0.87% of live MNE cells were MPIO+ and $CD11b^+$. Thus, other immune cells, aside from $CD3^+$ and $CD11b^+$ cells, can also take up MPIO, as, in this example, 0.35% of lymphocytes in the spleen were MPIO+ yet $CD3^-$. Likewise, more than half of the MPIO-labeled cells in the MNE gate were $CD11b^-$. In contrast, nearly all of the MPIO-labeled bone marrow cells in the MNE gate were $CD11b^+$.

The mean values of adjusted double-positive cells from all mice are shown in Table 1. Percentages were adjusted by subtracting values obtained with control samples (not shown). The percentage of MPIO+ cells that were $CD3^+$, $CD19^+$, or $CD11b^+$ in the respective gates is also presented. In the spleen, 0.57% ± 0.07 (mean ± standard deviation) of live lymphocytes were MPIO+. Of these MPIO-labeled lymphocytes, $CD3^+$ T cells accounted for 33.35% ± 4.03 and $CD3^+$/MPIO+ accounted for 0.19% ± 0.04. These values were higher in the bone marrow, as 0.31% ± 0.06 were $CD3^+$/MPIO+, with $CD3^+$ cells accounting for almost half (45.19% ± 4.85%) of the MPIO+ population.

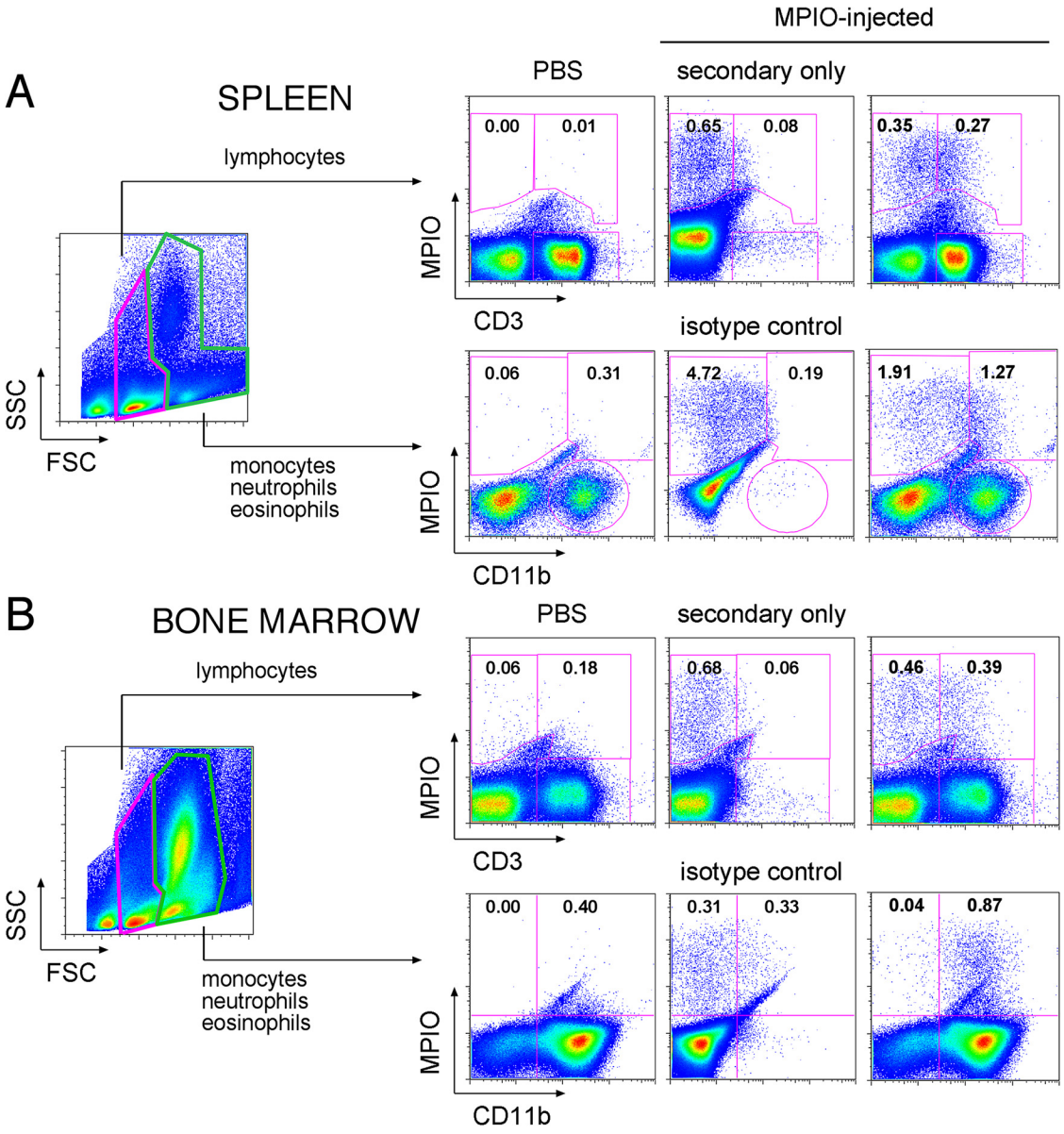

Figure 5. Flow cytometric assessment of MPIO-labeled immune cells in the spleen (A) and the bone marrow (B) 24 hours after MPIO injection. Plots from 1 representative MPIO-injected mouse are shown. From the live cell gate in forward scatter/side scatter, 2 broadly defined gates were set for lymphocytes and for combined monocytes, neutrophils, and eosinophils. Bangs Dragon Green fluorescence is indicated by "MPIO" on the y-axis; the T-cell marker CD3 and myeloid lineage marker CD11b are indicated on the x-axis. As negative controls, PBS plots (left column) show little or no fluorescence values pertaining to MPIO. Gates were set and values normalized based on secondary-only (for CD3) or isotype (for CD11b) controls (labeled panels in the middle column). The percent positive cells are indicated (right column). Background fluorescence values were subtracted from values obtained with fully stained samples to calculate percentages from which mean values are given in Table 1.

$CD19^+$ B cells comprised 51.47% of MPIO-labeled splenic lymphocytes at 0.28% ± 0.09% and only 12.38% of MPIO+ bone marrow lymphocytes at 0.05% ± 0.05%.

In the MNE gate, 3.00% ± 0.49 of live splenocytes were MPIO labeled. $CD11b^+$ cells accounted for 39.20% ± 5.27. The overall percentage of $CD11b^+$/MPIO+ was higher in the spleen than in the bone marrow (1.06% ± 0.16 vs 0.46% ± 0.13). In the bone marrow, however, $CD11b^+$ cells constituted the overwhelming majority of MPIO+ cells comprising 92.15% ± 3.48 of the total 0.50% ± 0.14 of MPIO-labeled bone marrow cells in the MNE gate. In summary, several types of immune cells, including T cells, B cells, and $CD11b^+$ myeloid cells, took up MPIO in the bone marrow and spleens of healthy MPIO-injected C57Bl/6 mice.

Table 1. Mean Values for Flow Cytometric Assessment of MPIO-Labeled Immune Cells in the Spleen and Bone Marrow

Gate	Spleen		Bone Marrow	
Lymphocyte	**Mean**	**SD**	**Mean**	**SD**
MPIO+	0.57	0.07	0.69	0.09
T cells: $CD3^+$ MPIO+	0.19	0.04	0.31	0.06
$CD3^+$ as % MPIO+	33.35	4.03	45.19	4.85
MPIO+	0.53	0.11	0.41	0.07
B cells: $CD19^+$ MPIO+	0.28	0.09	0.05	0.05
$CD19^+$ as % MPIO+	51.47	6.76	12.38	10.08
Monocyte/Neutrophil/Eosinophil				
MPIO+	3.00	0.49	0.50	0.14
$CD11b^+$MPIO+	1.06	0.16	0.46	0.13
$CD11b^+$ as % MPIO+	39.20	5.27	92.15	3.48
Total $CD11b^+$	31.26	2.51	84.55	5.02

Mean percentages and standard deviations (SD) obtained from the spleen and the bone marrow of 7 MPIO-injected mice are shown. In each box, MPIO+ is the total percentage of cells in the indicated gate (lymphocyte or monocyte/neutrophil/eosinophil) that were MPIO-labeled, as determined by acquisition of Dragon Green Fluorescence. The shaded line below this indicates the percentage of cells that were positive for both MPIO and the given marker. "% MPIO" is the percentage of the total MPIO+ population that also stained positive for this marker.

MRI of EAE Mouse Brain

Brain MRI of EAE mice revealed localized regions of signal loss in the brain in the images acquired 1 week after the onset of clinical signs of disease. Figure 6 shows representative MRI along with the corresponding F4/80-stained brain section. Punctate regions of signal loss appear in the brainstem in a pattern that can be matched with the F4/80 staining, indicating that the signal loss can be attributed to the presence of iron-labeled macrophages. Signal hypointensities were detected in 7/10 mice in images obtained 1 week after clinical signs and were typically located near ventricles, near the corpus callosum, and in the brainstem and cerebellum. No signal loss was detected in the brain images acquired 1 day after clinical signs.

DISCUSSION

Many studies have shown that circulating macrophages can be labeled by administration of a well-timed single bolus of iron oxide contrast agent in diseased animals, during ongoing or active inflammation, and that MRI can be used to detect these iron-labeled cells in inflammatory lesions (1-6, 9, 11-15, 20).

Others have explored the in vivo labeling strategy from a different perspective. It is possible to preload macrophages with iron particles in healthy animals and to subsequently induce an inflammatory disease and detect iron-positive cells that accumulate at the site of inflammation. For example, Henning et al preloaded rats with IV SPIO 1 week before inducing a stroke model, and the MRI showed signal loss at the lesion periphery 2–4 days poststroke (20). Immunohistochemistry showed that the signal loss in MR images corresponded with iron-positive central nervous system macrophages (20). Khurana et al have shown that IV administration of iron particles labels bone marrow-derived mesenchymal stem cells in vivo (21). This can be performed before harvesting mesenchymal stem cells for transplantation studies, and then the fate of these iron-labeled cells can be tracked by MRI (21). This is the first study that demonstrates preloading of specific cells in the mouse. We also applied this preloading strategy to detect cellular infiltration in a mouse model of MS. Mice were injected with SPIO 1 week before inducing EAE, and the images, acquired 1 week after signs of hindlimb weakness, showed distinct regions of signal loss in the brain that corresponded with F4/80 staining, confirming the presence of macrophages.

It was important to identify the types of immune cells, in which tissues were being labeled by iron particles administered

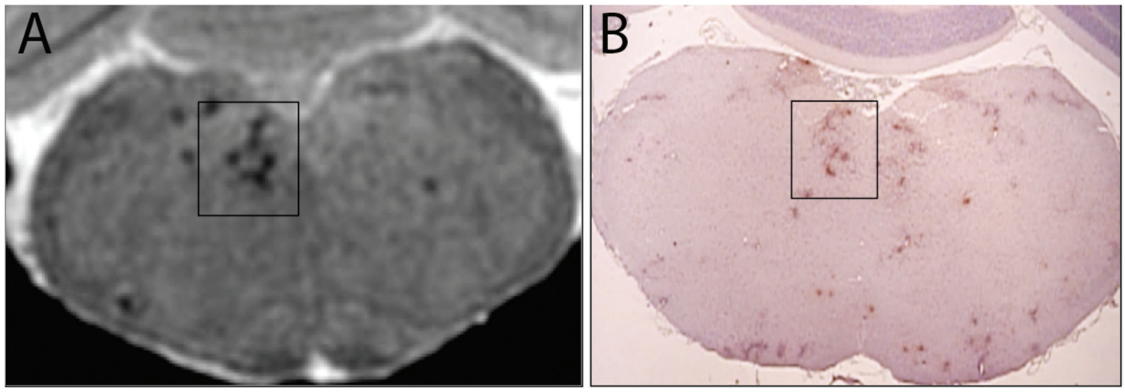

Figure 6. Balanced steady-state free precession image of EAE mouse brain (A) and corresponding F4/80-stained brain section (B), at the level of the brainstem. Regions of signal loss and those highlighted by the box in the brainstem image in (A) correspond well with the F4/80-stained regions in (B), indicating that the regions of signal loss can be attributed to the accumulation of iron-labeled macrophages. The mouse was administered SPIO IV 1 week before induction of EAE, and this image was obtained on day 23 postdisease induction when the signs of hindlimb paralysis were evident.

in this way. Because reservoirs of mobilizing immune cells have been recognized to also exist in the spleen (22), we analyzed the bone marrow and spleen using flow cytometry to sort for fluorescence associated with the MPIO label. The presence of positively labeled B cells, T cells, and monocytes within both the spleen and the bone marrow was confirmed. Considering both lymphocyte and MNE gates together, there were greater numbers of MPIO-positive cells in the spleen compared with the bone marrow, corroborating our histology and MRI data.

Although there were higher numbers of $CD11b^+$MPIO+ cells in the MNE gate in the spleen, it is interesting to point out that the splenic $CD11b^+$MPIO+ cells comprised less than half of all MPIO+ cells (39.20%), while, in the bone marrow, 92% of the MPIO+ population was $CD11b^+$. This is consistent with a higher percentage of $CD11b^+$ cells in the bone marrow overall, with 84.55% $CD11b^+$ cells in the MNE gate in the bone marrow compared with only 31.26% in the spleen (Table 1). Although often deemed a monocyte/macrophage marker, CD11b can also be found on neutrophils and granulocytes, as well as on the subsets of dendritic and natural killer cells. More specific identification of these subsets by flow cytometry would require the use of antibody cocktails encompassing several other markers.

In the bone marrow, roughly half of the MPIO+ cells in the lymphocyte gate were $CD3^+$ T cells. These cells also comprised approximately one-third of labeled cells in the spleen, showing that not only $CD11b^+$ cells take up MPIO in vivo. Other labeled cells in the bone marrow and the spleen included B cells, with $CD19^+$ cells accounting for just over half of MPIO+ cells in the spleen and ~12% of MPIO+ cells in the bone marrow (Table 1).

Tang et al previously investigated the in vivo labeling of bone marrow with IV MPIO (23). They showed that MPIO arrives in large quantities in the bone marrow following systemic delivery, as evidenced by the change in the MR signal, which agrees with our imaging data. However, their flow cytometric analysis of bone marrow cells showed that neither $CD11b^+$ cells nor $CD45^+$ cells were MPIO positive. The differences between our results and those of Tang et al may be due, in part, to differences in our experimental strategies. Although they used 4-week-old CD-1 mice, our study used 8- to 11-week-old C57Bl/6 mice. Differences in the neutrophil and monocyte compartments are evident when reviewing hematological data for these 2 strains. The numbers of circulating neutrophils (1.56 vs 1.19 K/μL) and monocytes (0.55 vs 0.36 K/μL) are substantially higher in 8- to 10-week-old CD-1 mice than in C57Bl/6 mice (24, 25). The larger number of circulating monocytes in CD-1 mice may mean that MPIO particles' uptake by these cells limits the amount of bone marrow labeling. Tang et al hypothesized that depletion of the circulating monocytes, which compete for MPIO, may facilitate in vivo labeling of bone marrow cells. In our study, isotype and secondary-only controls were used to carefully define the background for flow cytometry gating. The irregular SSC properties of labeled cells, because of MPIO, were taken into consideration when gating the lymphocyte and MNE populations for our analyses.

Thus, we have shown that cells in the mouse bone marrow and spleen take up iron particles after the IV administration of either SPIO or MPIO, and that this prelabeling of immune cells can be used to image the trafficking of cells into inflammatory lesions. The ability to prelabel a reservoir of cells that are considered to be mobilized from the spleen or the bone marrow at inflammation onset, with an MRI iron-based contrast agent, will allow for in vivo and longitudinal monitoring of their trafficking and fate in inflammation and injury models. In studies of inflammation where immune cells are rapidly dividing, the iron label will be diluted over time and, therefore, the length of time for which these cells may be tracked will be shortened. Nevertheless, this work sets the stage for future studies that aim to monitor the trafficking or recruitment of prelabeled immune cells from the spleen and the bone marrow in murine models of inflammatory disease and immune disorders.

ACKNOWLEDGMENTS

The Multiple Sclerosis Society of Canada provided grant funding for this research and provided studentship to S.K. The authors wish to thank Dr. Emeline Ribot for assistance with tail vein injections, Nikki Santyr and Chelsey Gareau for animal care and EAE scoring, and Drs. Andrew Alejski and Brian Rutt for the design and construction of the MR hardware used for this study. We thank Dr. Greg Dekaban and Dr. Kristin Chadwick at the London Regional Flow Cytometry Facility for their expert advice on flow cytometry. We also thank HJ and KM for their generous donation towards this research.

Conflict of Interest: None reported.

REFERENCES

1. Dousset V, Ballarino L, Delalande C, Coussemacq M, Canioni P, Petry KG, Caillé JM. Comparison of ultrasmall particles of iron oxide (USPIO)-enhanced T2-weighted, conventional T2-weighted, and gadolinium-enhanced T1-weighted MR images in rats with experimental autoimmune encephalomyelitis. AJNR Am J Neuroradiol. 1999 Feb;20(2):223–227.
2. Oweida AJ, Dunn EA, Karlik SJ, Dekaban GA, Foster PJ. Iron-oxide labeling of hematogenous macrophages in a model of experimental autoimmune encephalomyelitis and the contribution to signal loss in fast imaging employing steady state acquisition (FIESTA) images. J Magn Reson Imaging. 2007 Jul; 26(1):144–151.
3. Matsushita T, Kusakabe Y, Fujii H, Murase K, Yamazaki Y, Murase K. Inflammatory imaging with ultrasmall superparamagnetic iron oxide. Magn Reson Imaging. 2011 Feb;29(2):173–178.
4. Dardzinski BJ, Schmithorst VJ, Holland SK, Boivin GP, Imagawa T, Watanabe S, Lewis JM, Hirsch R. MR imaging of murine arthritis using ultrasmall superparamagnetic iron oxide particles. Magn Reson Imaging. 2001 Nov;19(9):1209–1216.
5. Dousset V, Gomez C, Petry KG, Delalande C, Caille JM. Dose and scanning delay using USPIO for central nervous system macrophage imaging. MAGMA. 1999 Aug;8(3):185–189.
6. Kleinschnitz C, Bendszus M, Frank M, Solymosi L, Toyka KV, Stoll G. In vivo monitoring of macrophage infiltration in experimental ischemic brain lesions by magnetic resonance imaging. J Cereb Blood Flow Metab. 2003 Nov;23(11):1356–1361.
7. Seyfer P, Pagenstecher A, Mandic R, Klose KJ, Heverhagen JT. Cancer and inflammation: differentiation by USPIO-enhanced MR imaging. J Magn Reson Imaging. 2014 Mar;39(3):665–672.
8. Zhang Y, Wells J, Buist R, Peeling J, Yong VW, Mitchell JR. Active inflammation increases the heterogeneity of MRI texture in mice with relapsing experimental allergic encephalomyelitis. Magn Reson Imaging. 2014 Feb;32(2):168–174.
9. Dousset V, Delalande C, Ballarino L, Quesson B, Seilhan D, Coussemacq M, Thiaudiére E, Brochet B, Canioni P, Caillé JM. In vivo macrophage activity imaging in the central nervous system detected by magnetic resonance. Magn Reson Med. 1999 Feb;41(2):329–333.

10. Wu YL, Ye Q, Foley LM, Hitchens TK, Sato K, Williams JB, Ho C. In situ labeling of immune cells with iron oxide particles: an approach to detect organ rejection by cellular MRI. Proc Natl Acad Sci U S A. 2006 Feb;103(6):1852–1857.
11. Yang Y, Yanasak N, Schumacher A, Hu TC. Temporal and noninvasive monitoring of inflammatory-cell infiltration to myocardial infarction sites using micrometer-sized iron oxide particles. Magn Reson Med. 2010 Jan;63(1):33–40.
12. Petry KG, Boiziau C, Dousset V, Brochet B. Magnetic resonance imaging of human brain macrophage infiltration. Neurotherapeutics. 2007 Jul;4(3):434–442.
13. Metz S, Beer AJ, Settles M, Pelisek J, Botnar RM, Rummeny EJ, Heider P. Characterization of carotid artery plaques with USPIO-enhanced MRI: assessment of inflammation and vascularity as in vivo imaging biomarkers for plaque vulnerability. Int J Cardiovasc Imaging. 2011 Jul;27(6):901–912.
14. Saleh A1, Schroeter M, Ringelstein A, Hartung HP, Siebler M, Mödder U, Jander S. Iron oxide particle-enhanced MRI suggests variability of brain inflammation at early stages after ischemic stroke. Stroke. 2007 Oct;38(10):2733–2737.
15. Gaglia JL1, Guimaraes AR, Harisinghani M, Turvey SE, Jackson R, Benoist C, Mathis D, Weissleder R. Noninvasive imaging of pancreatic islet inflammation in type 1A diabetes patients. J Clin Invest. 2011 Jan;121(1):442–445.
16. Crimi A, Commowick O, Maarouf A, Ferré JC, Bannier E, Tourbah A, Berry I, Ranjeva JP, Edan G, Barillot C. Predictive value of imaging markers at multiple sclerosis disease onset based on gadolinium- and USPIO-enhanced MRI and machine learning. PloS One. 2014 Apr;9(4):e93024.
17. Gaglia JL, Harisinghani M, Aganj I, Wojtkiewicz GR, Hedgire S, Benoist C, Mathis D, Weissleder R. Noninvasive mapping of pancreatic inflammation in recent-onset type-1 diabetes patients. Proc Natl Acad Sci U S A. 2015 Feb;112(7):2139–2144.
18. Yilmaz A, Dengler MA, van der Kuip H, Yildiz H, Rösch S, Klumpp S, Klingel K, Kandolf R, Helluy X, Hiller KH, Jakob PM, Sechtem U. Imaging of myocardial infarction using ultrasmall superparamagnetic iron oxide nanoparticles: a human study using a multi-parametric cardiovascular magnetic resonance imaging approach. Eur Heart J. 2013 Feb;34(6):462–475.
19. Xu S, Jordan EK, Brocke S, Bulte JW, Quigley L, Tresser N, Ostuni JL, Yang Y, McFarland HF, Frank JA. Study of relapsing remitting experimental allergic encephalomyelitis SJL mouse model using MION-46L enhanced in vivo MRI: early histopathological correlation. J Neurosci Res. 1998 Jun;52(5):549–558.
20. Henning EC, Ruetzler CA, Gaudinski MR, Hu TC, Latour LL, Hallenbeck JM, Warach S. Feridex preloading permits tracking of CNS-resident macrophages after transient middle cerebral artery occlusion. J Cereb Blood Flow Metab. 2009 Jul;29(7):1229–1239.
21. Khurana A, Chapelin F, Beck G, Lenkov OD, Donig J, Nejadnik H, Messing S, Derugin N, Chan RC, Gaur A, Sennino B, McDonald DM, Kempen PJ, Tikhomirov GA, Rao J, Daldrup-Link HE. Iron administration before stem cell harvest enables MR imaging tracking after transplantation. Radiology. 2013 Oct;269(1):186–197.
22. Swirski FK, Nahrendorf M, Etzrodt M, Wildgruber M, Cortez-Retamozo V, Panizzi P, Figueiredo JL, Kohler RH, Chudnovskiy A, Waterman P, Aikawa E, Mempel TR, Libby P, Weissleder R, Pittet MJ. Identification of splenic reservoir monocytes and their deployment to inflammatory sites. Science. 2009 Jul;325(5940):612–616.
23. Tang KS, Hann B, Shapiro EM. On the use of micron-sized iron oxide particles (MPIOS) to label resting monocytes in bone marrow. Mol Imaging Biol. 2011 Oct;13(5):819–824.
24. Charles River Laboratories. Clinical Pathology Data for North American CD-1 Mouse Colonies for January 2008 - December 2011.http://www.criver.com/files/pdfs/rms/cd1/rm_rm_r_cd1_mouse_clinical_pathology_data.aspx; last accessed 13 January 2016.
25. Charles River Laboratories. Charles River Laboratories. Biochemistry and Hematology for C57BL/6NCrl Mouse Colonies in North American for January 2008 - December 2012. http://www.criver.com/files/pdfs/rms/c57bl6/rm_rm_r_c57bl6_mouse_clinical_pathology_data.aspx; last accessed 13 January 2016.